J Mater Sci (2007) 42:6600–6606
DOI 10.1007/s10853-007-1501-5

Hardness and structural correlation for electroless Ni alloy deposits

M. Palaniappa · S. K. Seshadri

Received: 1 November 2006 / Accepted: 5 January 2007 / Published online: 26 April 2007

Abstract Electroless nickel (EN) plating has received attention as a hard coating for industrial applications due to its high hardness, uniform thickness as well as excellent corrosion and wear resistance. The electroless Ni–P deposit is a supersaturated alloy in as-deposited state, and can be strengthened by precipitation of nickel phosphide crystallites with suitable heat treatments. However, the hardness of Ni–P films degrades with excessive annealing due to grain coarsening. This is the most severe barrier for electroless Ni–P deposition process from replacing chromium plating in industrial sectors. This problem is addressed in the paper by modifying the conventional electroless Ni–P bath to co-deposit tungsten to increase the hardness of the coating. Structural changes in the coating due to incorporation of tungsten are also highlighted. Deposition is done from an alkaline hypophosphite bath. Deposits with varying tungsten content are synthesized. Chemical analysis shows that tungsten incorporation reduces the phosphorus content in the deposit. Phosphorus content varied from 3 to 7 wt.% depending upon the tungsten incorporation in the deposit which in turn varied between 8 and 18 wt.%. Coatings with high tungsten content possess high hardness when compared to binary Ni–P as well as low tungsten ternary alloy deposits.

M. Palaniappa · S. K. Seshadri
Department of Metallurgical and Materials Engineering, Indian Institute of Technology Madras, Chennai 600036, India

Present Address:
M. Palaniappa (✉)
NFTDC, Kanchanbagh Post, Hyderabad 500 058, India
e-mail: mpalaniappa@yahoo.com;

M. Palaniappa
mpalaniappa@nftdc.res.in

Introduction

Electroless nickel (EN) plating has found many applications in industry because of its deposit properties, such as its excellent corrosion and wear resistance, deposit uniformity, solderability etc [1, 2]. It has been shown that most of the properties of electroless nickel are structure-dependent and the structure is closely related to the phosphorus content of the coatings [3]. The phosphorus content of the deposit varies with pH of the bath [4]. Deposits plated from an alkaline solution have lower phosphorus content and are crystalline [5, 6], whereas deposits plated from an acidic bath contain high phosphorus and usually have an amorphous or a microcrystalline structure [7, 8]. On heating, the single phase electroless nickel crystallizes [9] (or rapid grain growth occurs from the microcrystalline structure) to a two phase mixture of Ni and Ni_3P as predicted by the Ni–P binary phase diagram [10]. At the same time the hardness and wear resistance of the deposit increases rapidly [11, 12]. Though electroless binary Ni–P alloys have had extensive application in industry due to their excellent wear and corrosion resistance and special physical performances, some ternary electroless alloys such as Ni–Cu–P [13, 14], Ni–Zn–P [15] and Ni–W–P [16–18] have also been developed to further enhance the properties of the binary system to meet more rigorous demands. Considerable work has been carried out to characterize binary electroless Ni–P alloy deposits [19] while the ternary systems have been studied to a much lesser

extent [20–22]. Very little work has been done to evaluate the structural and hardness of electroless Ni–W–P deposits. This paper makes an attempt fill this gap.

Experimental details

Coating was done on mild steel coupons of size 30 mm dia. and 5 mm thickness. Coating for obtaining foils was done on stainless steel plates. Due to the presence of passive film on the stainless steel plate, coating adhesion is very weak, aiding in easy peeling off of the coating. The sample is mechanically polished and degreased using trichloroethylene and thoroughly rinsed with deionised water, before actual deposition. The chemically cleaned coupons and plates were electrolytically cleaned using an aqueous alkaline solution having a composition of 25 g/L Na_2CO_3, 35 g/L NaOH and 1 g/L sodium lauryl sulphate at room temperature subjecting the samples initially as anode and later as cathode and then finally as anode for 20 s each applying a current of 5 A/dm^2. The electrolytically cleaned samples were then thoroughly rinsed in deionised water and were used for the electroless deposition after giving a nickel strike from a nickel sulphamate bath. Bath composition used for the electroless plating was nickel sulphate 30 g/L, sodium hypophosphite 14 g/L, sodium citrate 30 g/L, ammonium sulphate 30 g/L and sodium tungstate 0–20 g/L. Bath was operated at a pH of 8.5, time of deposition was 3 h at a bath temperature of 85 ± 2 °C. Chemical composition of the coating was determined using wet chemical method and further validation was done by Inductively Coupled Plasma-Atomic Emission Spectroscopy (ICP-AES). Plating rate was determined from the gain in weight of the sample after every hour of plating.

The structure of electroless nickel coatings largely depend on the alloying elements of the deposit which in turn is influenced by the type of plating bath used and its operating conditions. In order to determine the structure of electroless plated Ni–P and Ni–W–P deposits, both in as-plated and heat treated (300–600 °C for 1 h each) conditions, X-ray diffraction (XRD) measurements were made with a Shimadzu XD D1 diffractometer using CuK_α (λ = 1.54 Å) radiation. Microhardness measurements were made using Leitz Wetzlar microhardness tester with a Vickers indenter. A constant load of 100 g was applied for 20 s each to cause the indentations in all the deposits and the hardness values were averaged out of three such determinations. Thin foils of electroless Ni–P and Ni–W–P alloy deposits are employed for structural characterization by transmission electron microscopy (TEM). TEM study was performed using a Philips Transmission Electron Microscope (Model CM 12), operated at 120 KV.

Results and discussion

Plating rate and chemical composition

Plating rate of the deposits varied from 12 to 18 μm/h depending on the bath composition. Further, with time there is a reduction of plating rate. This is due to the depletion of metal ions and other reagents in the bath. Chemical composition of the coatings is given in Table 1. The nomenclature of the coatings as given in the table will be followed in this paper. Tungsten composition in the deposit was varied by adjusting the concentration of sodium tungstate in the bath. Bath containing highest amount of sodium tungstate possessed high plating rates. This is because of the addition of sodium tungstate in the bath, which acts as a complexing agent in addition to supplying tungsten metal ions for deposition. Gad and El-Magd [23] have suggested that addition of organic additives like sodium tungstate enhances the deposition rate at low concentrations, and this is attributed to the presence of an electron-attracting group which acts as a chelating agent for the formation of soluble nickel complexes. These complexes adsorb on the substrate surface and consequently enhance plating. This is also due to the increased ratio of metal ions to hypophosphite ions in the plating solution. With further additions (>20 g/L) of sodium tungstate, a decreasing trend in incorporation and deposition rate is observed due to spontaneous decomposition of the plating solution. Decomposition is usually initiated by the presence of colloidal solid nuclei in the solution or by increasing the concentration of hypophosphite or by increasing the temperature of deposition. In this work, increasing metal (tungsten) ion content (beyond 20 g/L tungstate) leads to self-accelerating chain reaction and decomposition. This is usually preceded by increased hydrogen evolution and the appearance of finely divided black precipitate throughout the solution. The precipitates mainly consist of nickel or nickel phosphide.

Structural aspects

Figure 1 show the XRD pattern for as plated electroless Ni–P and Ni–W–P deposits. The binary Ni–P is partially

Table 1 Chemical composition of Ni–P based alloy deposits

System*	Sodium tungstate concentration (g/L)	Chemical composition (wt.%)		
		Ni	W	P
8P1 (Ni–P)	0	93	–	7
8P2 (Ni–W–P)	4	86	8	6
8P3 (Ni–W–P)	20	79	18	3

* Nomenclature for coating systems used in this paper

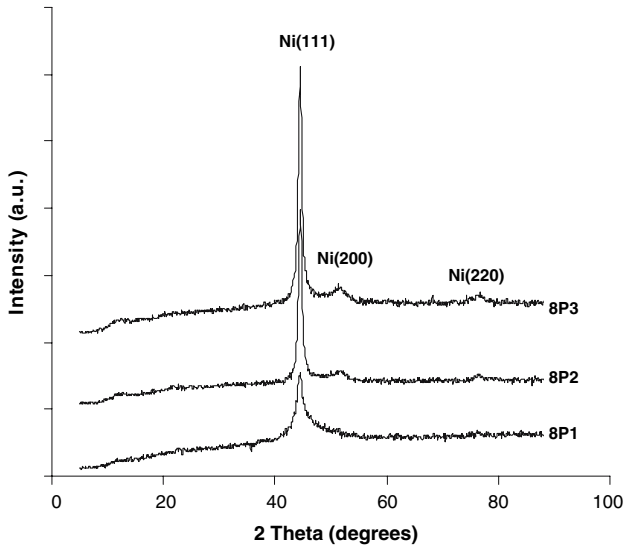

Fig. 1 XRD pattern of as-plated 8P deposits

crystalline in nature. The Ni (200) and Ni (220) peaks, other than the Ni (111) peak are clearly evident in the as-plated 8P2 and 8P3 deposits indicating their crystalline nature. Theoretically, a disorder in arrangement of atoms manifests itself as a broad peak in X-ray diffractograms [24]. The observed diffractogram of the electroless Ni–P deposit can be explained based on the mechanism of formation of these deposits. During electroless deposition, phosphorous atoms are randomly captured on the nickel atoms and the rate of segregation of these atoms determines the crystallinity of the deposit. Amongst these two atoms, the rate of diffusion of phosphorous is relatively small compared to that of nickel [25]. Hence, if the deposit contains higher amount of phosphorous, then a larger number of phosphorous atoms must be moved from a given area per unit time during deposition to achieve segregation of nickel and phosphorous.

It is observed that with increasing phosphorus content the (111) reflection from nickel becomes more broadened, indicating an increase in lattice disorder with increasing phosphorus content [26]. Xiang et al. [27] have obtained XRD data with varying phosphorus content in Ni–P deposit and observed that the coatings tend to show broadened peak above 7 wt.% phosphorus. Whereas, in this case the maximum phosphorus content in the deposit is 7 wt.% for 8P1 and reduces with increase in tungsten content. Thus the deposits 8P2 and 8P3 show more crystallinity compared to the binary alloy.

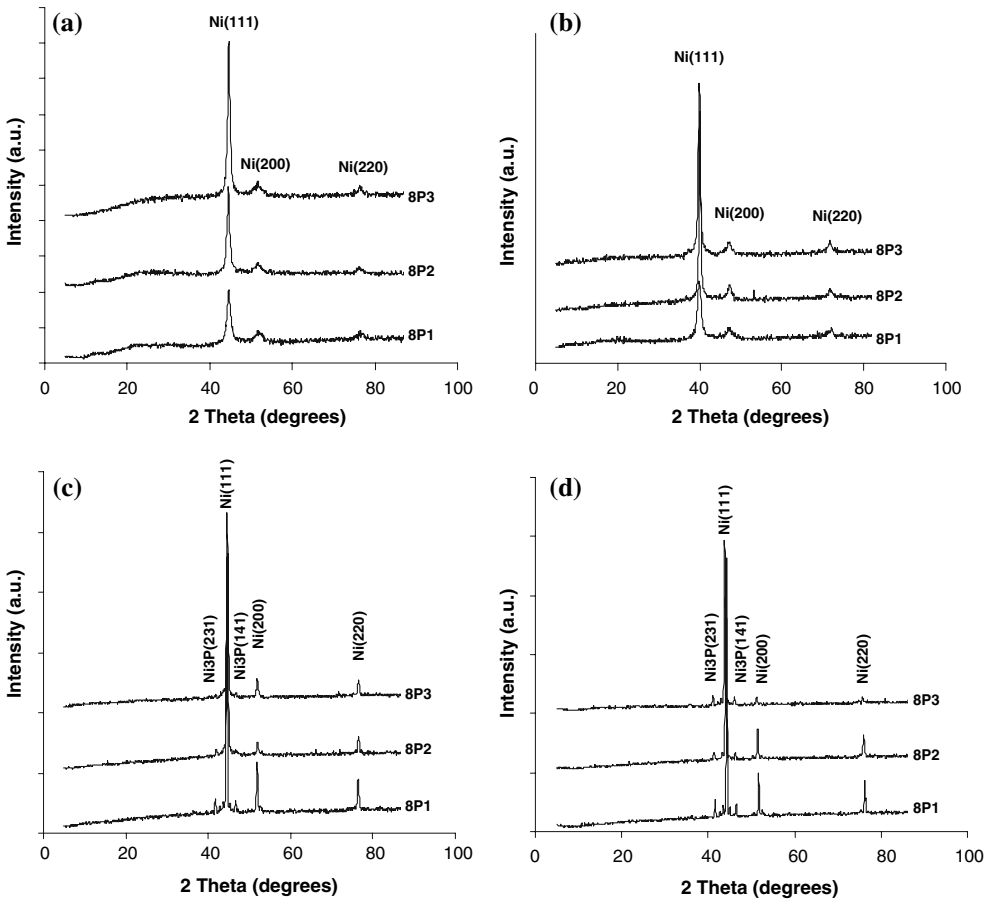

Fig. 2 XRD pattern of 8P coatings subjected to heat treatment at (**a**) 300 °C, (**b**) 400 °C, (**c**) 500 °C and (**d**) 600 °C for 1 h each

On heat treatment at 300 °C (Fig. 2a) for 1 h, 8P1 shows increased crystallinity and the Ni (200) and Ni (220) peaks are also visible in this case.

No phosphide peaks are visible, as the phosphorus content in the deposit is low and this temperature is not sufficient to precipitate the phosphide phases. The peaks remain unchanged even when annealed at 400 °C (Fig. 2b). The phosphide precipitation in this case is delayed for all the samples due to the reduced phosphorus content in the deposits.

The phosphide phases in the electroless deposition start becoming clearly visible after heating at 500 °C as shown in Fig. 2c. The reflections were indexed to be that of Ni_3P (231) and Ni_3P (141) phases. The intensities of the nickel peaks also have increased quite considerably after heating at 500 °C. The increased intensities of nickel peaks have further reduced the visibility of the phosphide peaks in 8P3. Upon heating the deposits at 600 °C (Fig. 2d), the precipitation of phosphides is clearly visible in all three deposits.

Intensities of the nickel peaks have increased considerably, indicating structural relaxation in the deposits [16]. The more intense nickel peaks in 8P1 and 8P2 is due to the higher amount of nickel present in the deposit.

Notable here is that, there is no reflection from tungsten or any tungsten compound in all the cases. This is due to the solid solution formation of tungsten in nickel matrix according to the binary Ni–W alloy phase diagram [28]. In Ni–W–P deposits, the tungsten incorporation impedes co-deposition of phosphorus atoms thereby reducing phosphorus content, which results in change in crystal structure.

X-ray diffraction forms a very powerful tool to study the structure and phases present in any system. However, it is very difficult to come to a definite conclusion with the XRD results alone and the data needs to be further validated by evaluation using a transmission electron microscope. Samples have been characterized using TEM wherein, diffraction patterns have been obtained with electron beam perpendicular to the surface of the thin film. Dark field and bright field imaging of the coatings were also done to study the microstructure of the coatings in detail, other than measuring the grain size of the coatings. TEM studies of only high tungsten deposits in both as-plated and heat treated condition have been highlighted here for discussing the structural aspects of the coatings. Figure 3 shows the TEM micrograph and diffraction pattern for as-plated 8P3. The partially crystalline nature of the deposit is clearly visible from the bright nickel spots scattered in between a hazy amorphous matrix. Diffraction pattern show three diffused rings of nickel.

The specimen (8P3) which exhibited one strong and two weak nickel peaks in the X-ray diffraction exhibits more than three strong diffraction rings in transmission electron microscopy giving an indication of a completely crystalline structure. The dark field image of the coatings give a very clear bright spots of Ni(111) which have size ranging from 5 to 15 nm. The number of diffraction rings is found to be very high when compared to the diffraction peaks from X-ray. This is because the crystallographic planes that are responsible for the appearance of a diffraction peak must be parallel to the surface of the specimen. An extremely strong (111) fibre texture perpendicular to the surface of a fcc metallic coating could cause destruction of all X-ray reflections except those from the {111} planes and similar higher order planes because these would be parallel to the surface of the specimen. The added effects of internal stress, solid solution, stacking faults and preferred orientation on the diminution of the intensities of the reflections can reasonably account for the destruction of all but the strong {111} X-ray reflection from the electroless coatings [18].

Appearance of any phosphide phase is not noticed on heating the sample at 300 and 400 °C (Fig. 4, 5, respectively). Delayed appearance of phosphide peaks is an indication of low phosphorus and also of the fact that tungsten in the deposit has a role in shifting phosphide precipitation to higher temperatures.

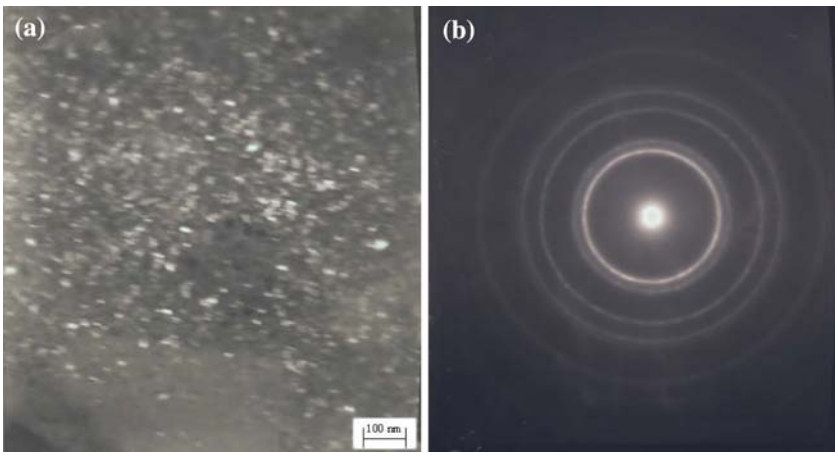

Fig. 3 TEM (**a**) darkfield micrograph and (**b**) diffraction pattern of as-plated 8P3

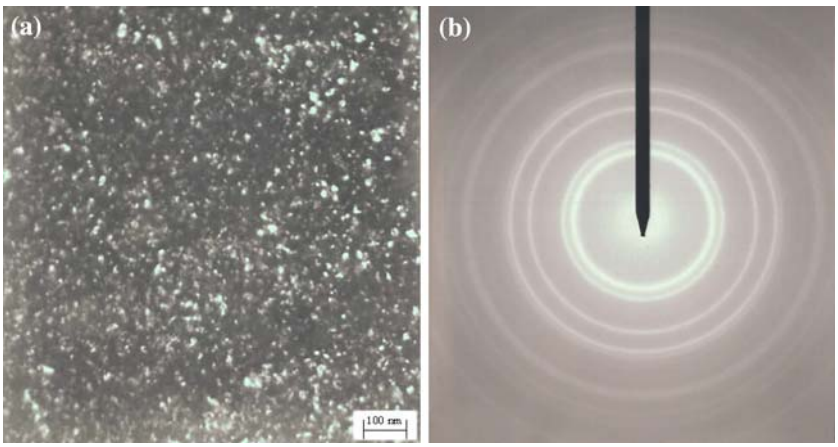

Fig. 4 TEM (**a**) darkfield micrograph and (**b**) diffraction pattern of heat treated (300 °C—1 h) 8P3

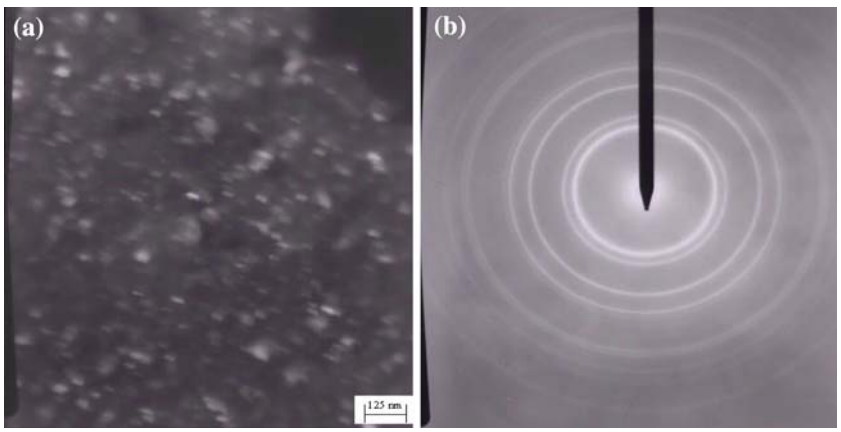

Fig. 5 TEM (**a**) darkfield micrograph and (**b**) diffraction pattern of heat treated (400 °C—1 h) 8P3

The increase in grain size of the deposits is also not significant for coatings heated at 500 °C (Fig. 6). There is clear evidence of the growth of Ni and Ni_3P phase in this case. Thus tungsten has an effect of providing high temperature stability to the coatings. The degree of effect increases with increase in the amount of tungsten.

Heating the electroless Ni–W–P coating at 600 °C leads to large grain growth as shown in Fig. 7. The dark field micrograph shows a non-uniform increase in the grain size. The diffraction rings dotted in nature indicating large grain growth.

Hardness

A major factor contributing to increased resistance to mechanical abrasion of electroless coatings is hardness.

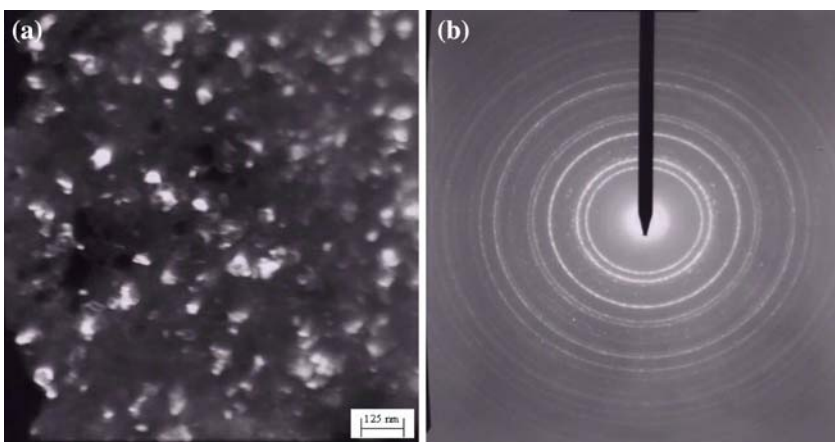

Fig. 6 TEM (**a**) darkfield micrograph and (**b**) diffraction pattern of heat treated (500 °C—1 h) 8P3

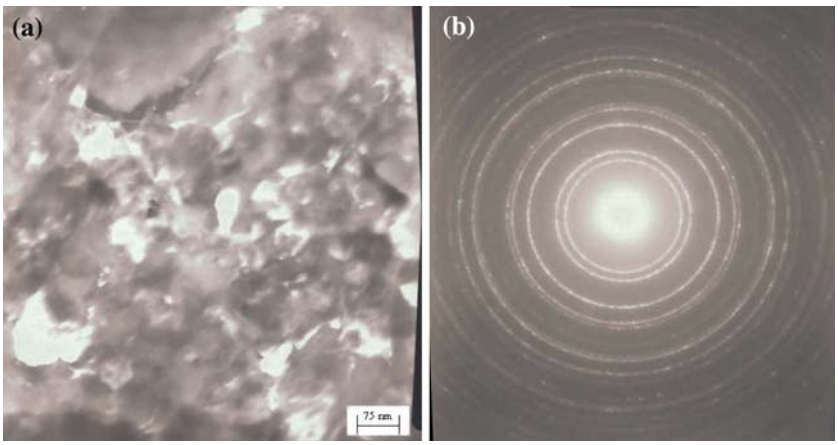

Fig. 7 TEM (**a**) darkfield micrograph and (**b**) diffraction pattern of heat treated (600 °C—1 h) 8P3

Despite different opinions regarding the structure of as-deposited electroless nickel coating as a function of phosphorus content, most of the investigators [29, 30] agree that electroless coatings when heat treated become crystalline due to the precipitation of phosphides. Precipitation of second phases leads to increased hardness in the coatings. Increased hardness in plain electrodeposited nickel is due to the presence of residual stresses and due to the reduced grain size in the coating. There is higher level of strain in the nickel matrix of electroless nickel deposit due to supersaturation of phosphorus. When electroless coatings are heated at suitable temperatures, precipitation of phosphides occurs which act as barriers for dislocation movement, thereby increasing the hardness further [31, 32].

The hardness of as-plated 8P1 is very low when compared to 8P2 and 8P3 (Fig. 8). The main reason for this behaviour is very low phosphorus content and absence of tungsten in the deposit. A considerable increase in the hardness values of deposits, with tungsten incorporation, is observed.

Upon heating the coatings at 300 °C, the hardness values increase in all the deposits. The increase in hardness has been attributed to fine Ni crystallites and hard intermetallic Ni_3P particles precipitated during the crystallization of the amorphous phase [8, 11, 29] in the case of binary Ni–P deposits and due to the solid solution strengthening of nickel by tungsten in the ternary alloy deposits.

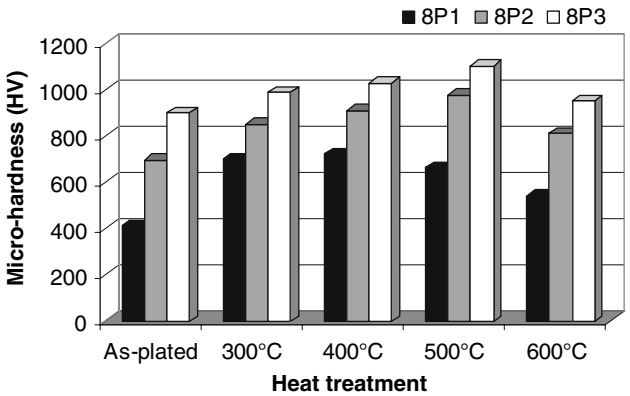

Fig. 8 Hardness profile for electroless Ni–P and Ni–W–P alloys from alkaline bath

When heated to very high temperatures there is a considerable increase in the sharpening of the peaks as seen in the X-ray and TEM diffraction pattern. This increased peak intensity is an indication of the increase in the size of crystallites of nickel and nickel phosphides. From the hardness study it is clear that contribution from solid solution strengthening in electroless nickel has a synergistic effect along with phosphide precipitation. Observation of increased hardness with increasing tungsten content was also made by Wu et al. [33] and Lin and Duh [34] in the case of sputtered Ni–P–W coatings. However, with increasing annealing temperatures the hardness values may decrease due to large grain growth. Peak hardness in binary alloys is attained on heating at 400 °C and on further heating (500 °C) is seen to decrease. In case of ternary alloy deposit the hardness is seen to increase even after heating beyond 400 °C and attains peak hardness of 1102VHN (8P3) after heating at 500 °C. The shift in the peak hardness to higher temperature compared to binary alloys could be due to the retarded precipitation of phosphide phases as a result of tungsten in the deposit as seen in XRD. On heating at higher temperatures (600 °C), the hardness values of Ni–W–P deposits also start decreasing. The reason is clearly visible from both XRD and TEM data, which show large grain growth for Ni–W–P coatings. Thus, from this study a very good correlation between the hardness values and structural aspect for electroless Ni–P and Ni–W–P has been observed.

Conclusions

Tungsten incorporation in Ni–P deposits result in lowering of phosphorus content, which in turn makes the deposits

more crystalline in nature. Phosphide precipitation upon heating is also delayed in the case of ternary alloys. Hardness values were seen to increase with increase in tungsten content in the deposit. The hardness values for Ni–W–P deposits in optimized heat treated conditions can be comparable to electrodeposited chromium.

References

1. Mallory GO, Hadju JB (1990) Electroless plating. AESF, Orlando, FL
2. Riedel W (1991) Electroless nickel plating. Finishing Publishers Ltd, England
3. Keong KG, Sha W (2002) Surf Eng 18:329
4. Shipley CR Jr (1984) Plating Surf Finish 71(6):92
5. Keong KG, Sha W, Malinov S (2004) Mater Sci Eng A 365:212
6. Sugita K, Ueno N (1984) Mater Sci Eng A 131:111
7. Keong KG, Sha W, Malinov S (2002) J Alloys Compd 334:192
8. Keong KG, Sha W, Malinov S (2001) Acta Metall Sin (English Letters) 14:419
9. Martyak NM, Wetterer S, Harrison L, Mcneil M, Heu R, Neiderer AA (1993) Plating Surf Finish 80(3):60
10. Hansen M (1965) Constitution of binary alloys. McGraw Hill Book Company, New York
11. Kanani N (1991) Trans IMF 70(1):14
12. Staia MH, Puchi ES, Castillo EJ, Lewis DB, Hintermann HE (1996) Surf Coatings Technol 86/87:598
13. Chen CJ, Lin KL (1999) J Electrochem Soc 146(1):137
14. Armyanov S, Steen O (1996) J Electrochem Soc 143(11):3692
15. Schlesinger M, Meng X (1990) J Electrochem Soc 137(6):1858
16. Zhang BW, Hu WY, Qu XY (1996) Mater Characterisation 37:119
17. Balaraju JN, Millath Jahan S, Jain A, Rajam KS (2006) J Alloys Compd. DOI: 10.1016/j.jallcom.2006.07.045
18. Hu Y-J, Wang T-X, Meng J-L, Rao Q-Y (2006) Surf Coatings Technol 201:988
19. Martyak NM, Drake K (2000) J Alloys Compd 312:30
20. Sankaranarayanan TSN, Selvakumar S, Stephen A (2003) Surf Coatings Technol 172:298
21. Yu H-S, Luo S-F, Wang Y-R (2001) Surf Coatings Technol 148:143
22. Tsai Y-Y, Wu F-B, Chen Y-I, Peng P-J, Duh J-G, Tsai S-Y (2001) Surf Coatings Technol 146–147:502
23. Gad MR, El-Magd A (2001) Met Finish 99(2):77
24. Warren BE (1969) X-ray diffraction. Addison-Weseley Publishing Company, Reading, MA
25. Szasz A, Fabian DJ, Paal Z, Kojnok J (1988) J Non-Cryst Solids 103:21
26. Allen RM, Vander Sande JB (1982) Scr Metallur 16:1161
27. Xiang Y, Hu W, Liu X, Luo S (2001) Plating Surf Finishing 88(6):96
28. American Society for Materials (1991) ASM handbook, volume 3 ''Alloy phase diagrams''. American Society for Materials, Material Park, OH
29. Kumar PS, Nair PK (1996) J Mater Process Technol 56(1–4):511
30. Keong KG, Sha W, Malinov S (2002) J Mater Sci 37:4445
31. Baudrand D, Bengston J (1995) Met Finishing 93(9):55
32. Barker D (1993) Trans Inst Met Finishing 71(3):121
33. Lin C-H, Duh J-G (2004) Surf Coatings Technol 188–189:495
34. Wu F-B, Chen Y-I, Peng P-J, Tsai Y-Y, Duh J-G (2002) Surf Coatings Technol 150:232